Pergamon

PII: S0191-8141(97)00062-X

Journal of Structural Geology, Vol. 19, No. 12, pp. 1443 to 1459, 1997

0191-8141/97 $17.00 + 0.00

Roof sequence response to emplacement of the Wills Mountain duplex: the roles of forethrusting and scales of deformation

KEVIN J. SMART* and WILLIAM M. DUNNE

Department of Geological Sciences, University of Tennessee, Knoxville, TN 37996-1410, U.S.A.

and

RAYMOND D. KRIEG

Department of Mechanical and Aerospace Engineering and Engineering Science, University of Tennessee, Knoxville, TN 37996-2030, U.S.A.

(*Received* 2 *April* 1997; *accepted in revised form* 11 *August* 1997)

Abstract—This paper focuses on the behavior of a roof sequence in the Appalachian Plateau of West Virginia, U.S.A., and emplacement of the Wills Mountain duplex with 17.5 km of displacement. Unlike the Plateau along strike in Pennsylvania and New York where forethrusting was previously documented, this roof sequence lacks an underlying salt-dominated roof décollement. Kinematic analyses reveal that the roof sequence in the West Virginian Plateau accommodated about two-thirds of the 17.5 km of shortening by the adjacent Wills Mountain duplex, as a forethrusting kinematic response. The remaining shortening imbalance of about 5 km between the duplexes and younger roof sequence rocks is accommodated by additional forethrusting further into the foreland and local compensation. This kinematic response matches that along strike in the central Appalachians despite the loss of the salt décollement. We interpret that an Ordovician shale-dominated formation was sufficiently weak to substitute for the salt horizon. Thus, a weak mechanical unit rather than specifically a salt décollement is a necessary prerequisite for forethrusting. A contributing factor to forethrusting may be the subvertical front of the Wills Mountain duplex, which inhibited other responses by the roof sequence. Mesoscale and smaller processes, including grain-to-grain pressure solution, twinning and cleavage formation account for over 75% of the shortening in the roof sequence, and, if ignored, would result in an erroneous interpretation of backthrusting or local compensation. This result suggests that failure to consider all deformation scales could lead to incorrect kinematic conclusions in other tectonic systems. © 1997 Elsevier Science Ltd.

INTRODUCTION

Blind foreland thrust systems are a common component of orogenic belts throughout the world (e.g. the Appalachians, Canadian Rockies, Taiwan, Norway, Pakistan, Bolivia and Alaska). A major unresolved problem with the development of duplexes is the interplay of the kinematic responses in the rocks above and in front of the duplexes. These rocks accommodate duplex formation, but are not part of the fault system because they are decoupled across the roof thrust of the duplex (Geiser, 1988a,b). Three end-member kinematic responses (Fig. 1) are possible (Banks and Warburton, 1986; Dunne and Ferrill, 1988; Geiser, 1988a,b; Ferrill and Dunne, 1989; Groshong and Epard, 1992): (1) *forethrusting* where rocks in the roof sequence deform in advance of the duplex and are transported into the foreland, compensating for duplex emplacement; (2) *backthrusting* where the roof sequence passively rides over and into the hinterland relative to the advancing duplex; and (3) *local compensation* where deformation in the roof sequence is concentrated above horses without a dominant transport direction towards the hinterland or foreland.

Forethrusting (Fig. 1a) occurs when the roof sequence remains coupled to the underlying duplex and is carried forward during deformation. Forethrusting has been proposed for blind thrust systems in the central Appalachians (Perry, 1978; Geiser and Engelder, 1983; Mitra, 1986; Geiser, 1988a,b; Ferrill and Dunne, 1989), Norway (Morley, 1986, 1987) and the eastern MacKenzie Mountains, Canada (Vann *et al.*, 1986). Forethrusting has been found to cause deformation at all scales in the roof sequence (Geiser and Engelder, 1983; Mitra and Yonkee, 1985; Geiser, 1988a,b; Ferrill and Dunne, 1989; Protzman and Mitra, 1990; Mitra, 1994; Dunne, 1996; McNaught and Mitra, 1996). The predicted effects of this response are: (1) foreland-verging structures including folds, thrusts and foliation that precede formation of blind macrostructures; and (2) a progressive decrease in deformation in the roof sequence toward the foreland beyond blind thrusts (Dunne and Ferrill, 1988; Geiser, 1988a,b; Gray and Mitra, 1993).

Backthrusting (Fig. 1b) occurs where the roof sequence is pinned in advance of the duplex but is able to decouple above the structure (Banks and Warburton, 1986; Dunne and Ferrill, 1988; Geiser, 1988a,b). Many cross-sections for blind foreland thrust systems incorporate backthrusting of the roof sequence explicitly or implicitly (Thompson, 1979, 1982; Price, 1981; Jones, 1982; Suppe, 1983;

* Author to whom correspondence should be addressed at: School of Geology and Geophysics, 810 Sarkeys Energy Center, University of Oklahoma, Norman, OK 73019-0628, U.S.A.

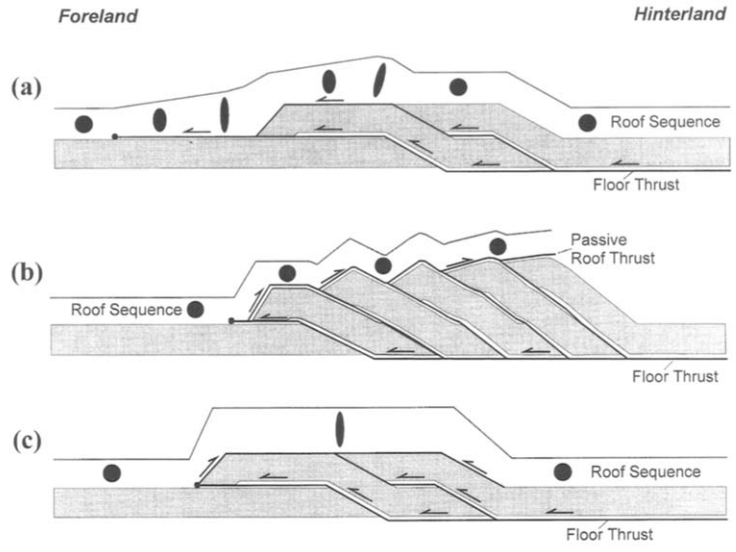

Fig. 1. End-member kinematic responses to emplacement of a blind thrust system. (a) Forethrusting, (b) backthrusting and (c) local compensation. Ellipses show location and intensity of micro- and mesoscale strain.

McMechan, 1985; Banks and Warburton, 1986; Vann *et al.*, 1986; Humayon *et al.*, 1991; Baby *et al.*, 1992; Jadoon *et al.*, 1994a,b). Backthrusting is treated by virtually all workers as a dominantly macroscale behavior where the roof sequence remains relatively stationary as the duplex is emplaced underneath. The predicted effects are: (1) hinterland-verging structures in the roof sequence; (2) little deformation in the roof sequence in front of the duplex; and (3) relative hinterland displacement of the roof, perhaps coupled with erosion, compensating for the apparent shortening discrepancy between the roof sequence and duplex (Banks and Warburton, 1986).

Local compensation (Fig. 1c) occurs where the roof sequence is decoupled above the duplex and deforms locally rather than being regionally transported. Local compensation has been proposed as a partial or complete response for several foreland thrust belts (Ferrill and Dunne, 1989; Wallace and Hanks, 1990; Groshong and Epard, 1992, 1994; Wu, 1993). The predicted effect is deformation in the roof sequence, which is concentrated directly above duplexes and is a direct function of the shortening in that particular duplex (Dunne and Ferrill, 1988; Groshong and Epard, 1992; Wu, 1993).

We document a case where a forethrusting response dominated the deformation of the roof sequence. Although this example comes from the central Appalachians where previous workers identified forethrusting behavior (Perry, 1978; Geiser and Engelder, 1983; Mitra, 1986; Geiser, 1988a,b; Ferrill and Dunne, 1989), this case is different because the roof flat is not in a salt décollement (Fig. 2). A central question, then, is whether along strike in the same foreland thrust belt we should expect the same kinematic response to blind thrusting if a very weak décollement horizon such as salt disappears? And if so, why?

We also evaluate the importance of the various scales of deformation to the total roof sequence shortening. The

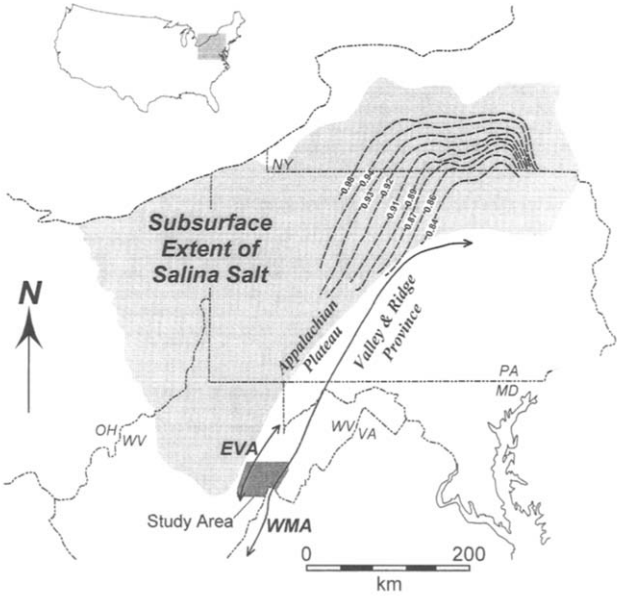

Fig. 2. Map showing distribution of Silurian Salina salt in the central Appalachians (Clifford, 1973). Heavy dashed lines are isostrain contours ($1+\epsilon_3$) modified from Geiser (1988a, fig. 2). EVA is Elkins Valley anticline and WMA is Wills Mountain anticline.

scales of observation are macroscale, mesoscale and microscale. Our size division between macroscale and mesoscale is 100 m because structures of this size can be clearly represented on our 1:24 000 base maps, and because most exposures with mesoscale (outcrop-scale) structures do not exceed this size. Microscale data were gathered from thin sections and individual crinoid columnals.

Macroscale deformation is typically assumed to be the largest component of deformation as geological cross-sections by their nature portray only map-scale structures. Recently, however, studies have demonstrated that a large percentage of roof sequence shortening is by

structures at a scale of tens of centimeters or less (Engelder and Engelder, 1977; Geiser and Engelder, 1983; Herman, 1984; Mitra and Yonkee, 1985; Geiser, 1988a,b; Ferrill and Dunne, 1989; Protzman and Mitra, 1990; Mitra, 1994; Dunne, 1996; McNaught and Mitra, 1996). This has profound implications for evaluation of kinematic responses. For example, the lack of macroscale structures in the foreland beyond a duplex is insufficient evidence for concluding that forethrusting is absent, and that only a combination of backthrusting and local compensation occurred. Even though measuring smaller scales of deformation is time consuming (Ramsay, 1967; Dunnet, 1969; Groshong, 1972, 1974; Groshong *et al.*, 1984a; Fry, 1979; Erslev, 1988; Schultz-Ela, 1990; Evans and Groshong, 1994), this contribution will again demonstrate the necessity of doing it and show the implications of the failure to consider smaller scale deformation.

GEOLOGICAL SETTING

The study area in central–east West Virginia (Fig. 3) is part of the classic central Appalachian blind foreland thrust belt that developed during the late Paleozoic Alleghanian orogeny (Rodgers, 1963, 1970; Gwinn, 1964; Perry, 1978; Geiser and Engelder, 1983). Thrust geometry consists of duplexes containing Cambro-Ordovician carbonates with a floor thrust in the Lower Cambrian Waynesboro–Rome Formation and a roof thrust in the Middle–Upper Ordovician Martinsburg Formation (Rodgers, 1963, 1970; Gwinn, 1964; Perry, 1978; Kulander and Dean, 1986; Mitra, 1986; Wilson and Shumaker, 1992). The study area extends northwestward from the northwestern limb of the Wills Mountain anticline to the northwestern limb of the Elkins Valley anticline (Figs 2 & 3). The deformed stratigraphy in the surface and subsurface ranges from the Waynesboro Formation to the Pennsylvanian Pottsville Group (Fig. 3). This area was chosen because: (1) the surface geology is well mapped (Tilton *et al.*, 1927; Price, 1929; Price and Heck, 1939; Cardwell *et al.*, 1968); (2) unpublished proprietary seismic reflection profiles and well data (Gwinn, 1964; Patchen *et al.*, 1977; Cardwell, 1982) are available to help constrain subsurface interpretations; (3) several stratigraphic units can be used to measure micro- to macroscale strain; and (4) a roof sequence is present above and adjacent to duplexes.

MACROSCALE SHORTENING IMBALANCE

The most distal major duplex in the central Appalachians, the Wills Mountain duplex (WMD, Fig. 4), accommodated 17 km of displacement in a flat-on-flat offset of Cambro-Ordovician carbonates (Wilson and Shumaker, 1992). This structure bounds the southeastern side of the study area with the surface expression of its hangingwall ramp cutoff, the Wills Mountain anticline (Figs 3 & 4). Beyond Wills Mountain to the northwest, the only other imbrication of the Cambro-Ordovician carbonates in the Appalachian Plateau is a single horse under the Elkins Valley anticline (Fig. 4) with approximately 0.5 km of displacement (Kulander and Dean, 1986; Wilson and Shumaker, 1988). Thus, any shortening greater than 0.5 km in roof sequence of the study area

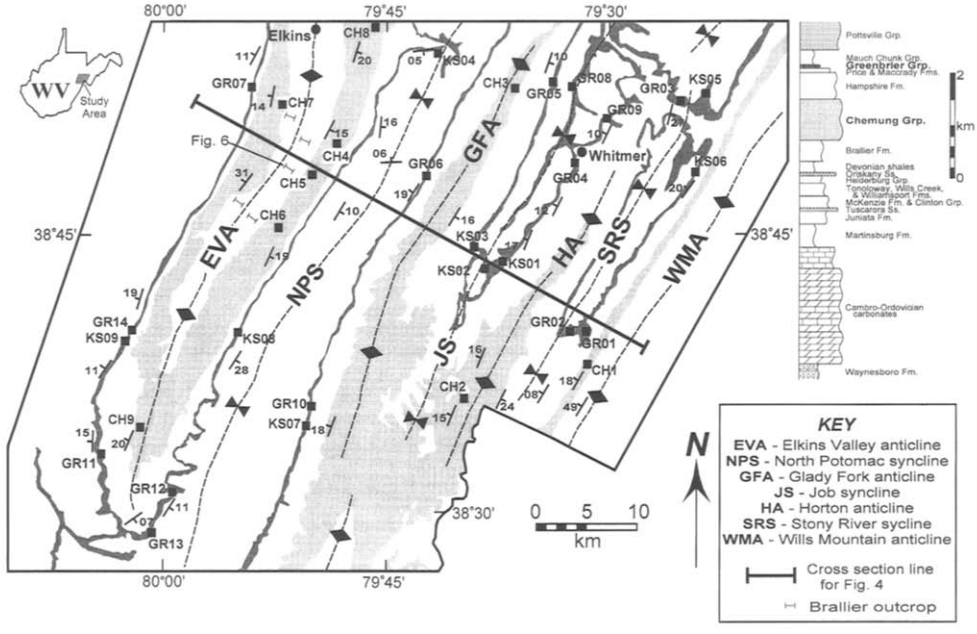

Fig. 3. Geological map of central–east West Virginia showing outcrop belts of Mississippian Greenbrier and Devonian Chemung Groups in the Appalachian Plateau. Sample locations (solid squares) are identified with sample numbers and representative bedding orientations are given.

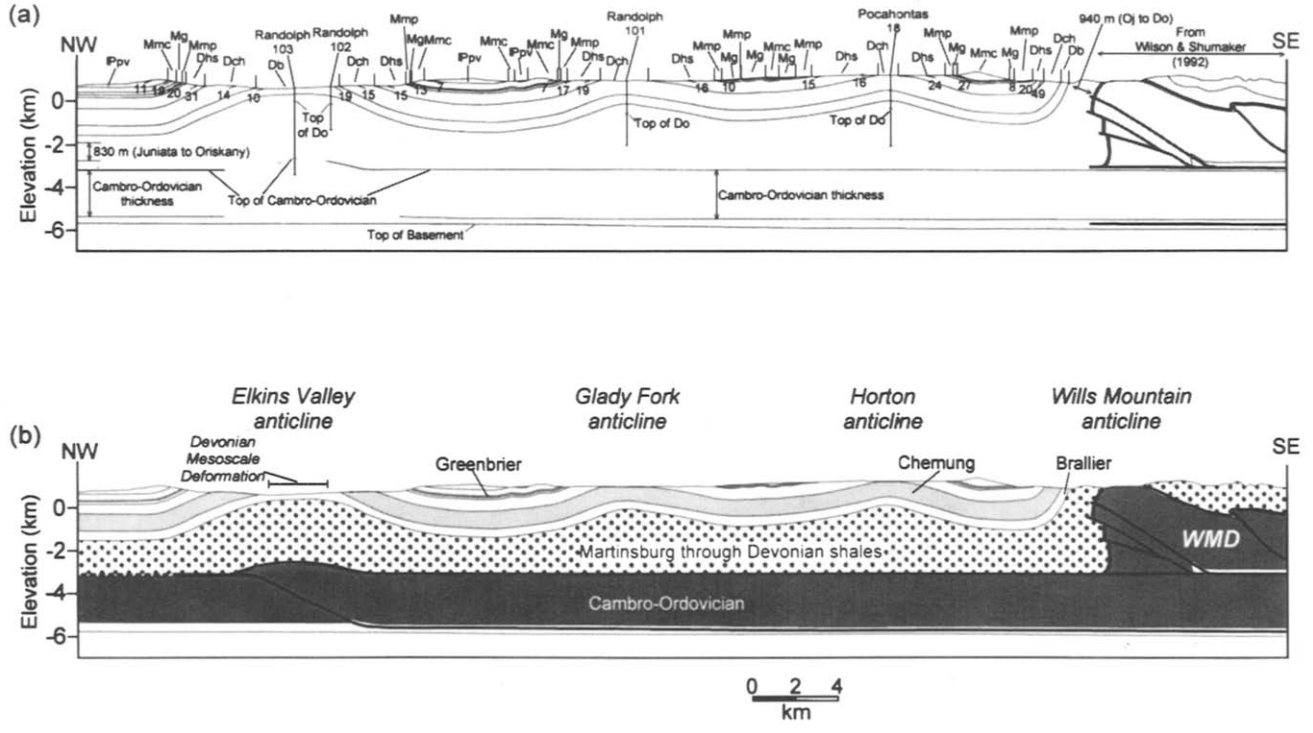

Fig. 4. (a) Illustration of constraints used in construction of a geological cross-section. (b) Geological cross-section across the study area. Tick marks with numbers indicate apparent dip in the plane of section.

would not represent an accommodation of duplex formation in the Plateau. Instead, the shortening must represent an accommodation of duplex(es) displacement from the hinterland and by definition is a forethrusting response by the roof sequence. The immediately adjacent duplex in the hinterland is the Wills Mountain duplex with its 17 km of displacement. The next duplex into the hinterland is the North Mountain duplex (NMD), which is about 50 km further to the southeast and has about 60 km of displacement (Wilson and Shumaker, 1988; Evans, 1989; Evans and Dunne, 1991; Dunne, 1996). Evans (1989,1990, 1997) has convincingly demonstrated that the majority of the displacement for the NMD is transferred through the surface trace of the North Mountain thrust and not into the foreland of the Appalachian Valley and Ridge, and Plateau. Consequently, if significant deformation was found in the roof sequence of the study area, it would represent an accommodation of the Wills Mountain duplex. This accommodation would be forethrusting because the roof sequence rocks are forelandward of the duplex.

A geological cross-section (Fig. 4) for the study area was constructed to estimate macroscale shortening. The cross-section is constrained (Fig. 4a) by the surface geological contacts and structural geometries (Tilton *et al.*, 1927; Price, 1929; Price and Heck, 1939; Cardwell *et al.*, 1968; unpublished mapping), published stratigraphic thickness (Tilton *et al.*, 1927; Price, 1929; Price and Heck, 1939; Reger, 1931; Woodward, 1941,1943,1949, 1951; Dennison and Naegele, 1963; Arkle, 1974; Smosna and Patchen, 1978; Smosna *et al.*, 1978; Arkle *et al.*, 1979; de Witt and McGrew, 1979; Cardwell, 1982; Carney, 1987; Adamson, 1992), depth-to-basement estimates (Kulander and Dean, 1986; Wilson and Shumaker, 1988, 1992; Adamson, 1992), proprietary seismic reflection data for the top of the Cambro-Ordovician carbonates and basement, and wells (Gwinn, 1964; Patchen *et al.*, 1977; Cardwell, 1982).

The macroscale structural style above the Devonian shales consists of a series of open anticline–syncline pairs with wavelengths of 14–16 km and amplitudes of less than 4 km (Figs 3 & 4). Macroscale shortening for the Middle Devonian–Pennsylvanian interval was measured as line-length changes (Dahlstrom, 1969; De Paor, 1988; Woodward *et al.*, 1989) because field observations demonstrate that bedding thickness is preserved. Across the study area macrofolding accounts for 2.4 km of roof sequence shortening in the Devonian and younger rocks (Table 1). The Cambro-Ordovician carbonates are also presumed to maintain bedding thickness based on proprietary seismic data for the study area (Fig. 4a) and observations outside the study area (Perry, 1978; Evans, 1989). As such, a line-length shortening value of 0.5 km was determined for the study area in addition to the 17 km present within the Wills Mountain duplex (Table 1 and Fig. 4).

The macroscale geometry of the interval from the Martinsburg Formation through to the Devonian shales is the least constrained portion of the deformed roof sequence because: (1) it is not exposed at the surface except in the steep forelimb of the Wills Mountain anticline; (2) it is not penetrated by many wells; and (3)

Table 1. Summary of shortening estimates within study area

Stratigraphic level	Individual shortening estimates: Microscale (km)	Mesoscale (km)	Macroscale (km)	Total shortening (km)	Missing shortening (km)
Greenbrier	6.2	3.3	2.4	11.9	5.6
Chemung	6.3	1.2	2.4	9.9	7.6
Ordovician–Devonian		←15.3→		15.3	2.2
Cambro-Ordovician	n.a.	n.a.	17.5	17.51*	n.a.

*Shortening value consists of 17 km in the Wills Mountain duplex and 0.5 km under the Elkins Valley anticline.
n.a., not applicable.

it is only partially imaged in the proprietary seismic reflection data (Fig. 4a). Northwest of Elkins Valley anticline, the proprietary seismic reflection profile reveals well-organized continuous horizontal reflectors for the Juniata Formation through to the Oriskany Sandstone, with a thickness of approximately 830 m (Fig. 4a). In contrast, this interval from the southeast limb of Elkins Valley anticline to the northwest limb of the Wills Mountain anticline has a thickened package of short, discontinuous, horizontal and inclined reflectors. This appearance indicates that the geometry is not characterized by macroscale thrusts or folds that deform the entire stratigraphic interval because such geometries would show panels of uniformly dipping reflectors. Rather, deformation is accommodated by structures less than 1 km long. This interpretation is consistent with recent work by Dunne (1996) that demonstrated the rarity of macroscale thrusts in the Ordovician and younger roof sequence in the Valley and Ridge province. The absence of easily resolvable large-scale structures in this stratigraphic interval means that the most honest way to treat shortening is to identify the area the rocks occupy (Fig. 4b) and determine shortening by area balance. An undeformed thickness of 1730 m was estimated for the Martinsburg–Millboro interval (Tilton *et al.*, 1927; Price, 1929; Reger, 1931; Smosna and Patchen, 1978; Smosna *et al.*, 1978; Cardwell, 1982; Adamson, 1992). An area of 113 km^2 was measured for this interval from the cross-section. Assuming plane strain and no volume loss, the initial thickness of 1730 m when divided into the deformed area (Chamberlain, 1910; De Paor, 1988; Woodward *et al.*, 1989; Mitra and Namson, 1990; Groshong and Epard, 1994) yields an undeformed section length of 65.3 km, or 15.3 km of shortening across the 50-km wide study area (Table 1). Unfortunately, the use of a macroscale area balance with no additional information from smaller scales means that the estimate of deformation for this interval cannot be partitioned as a function of scale.

Middle Devonian and younger rocks shortened by only 2.4 km at the macroscale compared to the duplexes in the Cambro-Ordovician carbonates, which shortened by 17.5 km. This imbalance may indicate that the roof sequence accommodated duplex formation by deformation at less than macroscale in the Middle Devonian and younger rocks or that kinematic responses outside the area accommodated duplex formation. A meso- to microscale analysis of the Devonian Chemung and Mississippian Greenbrier Groups was undertaken to assess the role of sub-macroscale deformation.

MESOSCALE STRAIN ASSESSMENT

Outcrop-scale deformation in Devonian rocks

Mesoscale folds and faults in Devonian rocks are restricted to a zone in the Brallier Formation in the core of the Elkins Valley anticline (Figs 3, 4b, 5a & 6). This zone is approximately 3 km wide (Fig. 4b), centered on the anticlinal hinge and present along the length of the anticline in the Devonian rocks. The transition between the folded and faulted Brallier Formation in the core of Elkins Valley anticline (Fig. 5a) and the uniformly dipping Brallier Formation and Chemung Group (Fig. 5b) occurs over a distance of a few tens of meters and is marked by the last occurrence of folded Brallier Formation. Mesoscale deformation is absent elsewhere in the Brallier Formation or Chemung Group of the study area, including the limbs of the Elkins Valley anticline.

Based on five profiles (Fig. 3), and a dozen other outcrops across the zone, mesoscale shortening by folds and faults is typically 40–50% (Figs 5a & 6). For example, a 200-m long outcrop (Figs 3 & 6) shows a shortening of 41%. Assuming a minimum of 40% shortening across the entire 3-km wide zone, mesoscale folding and faulting accommodates at least 1.2 km of shortening in the Devonian Brallier Formation in the core of Elkins Valley anticline. By lithological similarity, stratigraphic proximity and analogy, the eroded Chemung Group stratigraphically above the Brallier Formation is assumed to contain the same magnitude of shortening.

Greenbrier cleavage shortening

Limestones of the Mississippian Greenbrier Group are well exposed in the syncline limbs and cores throughout

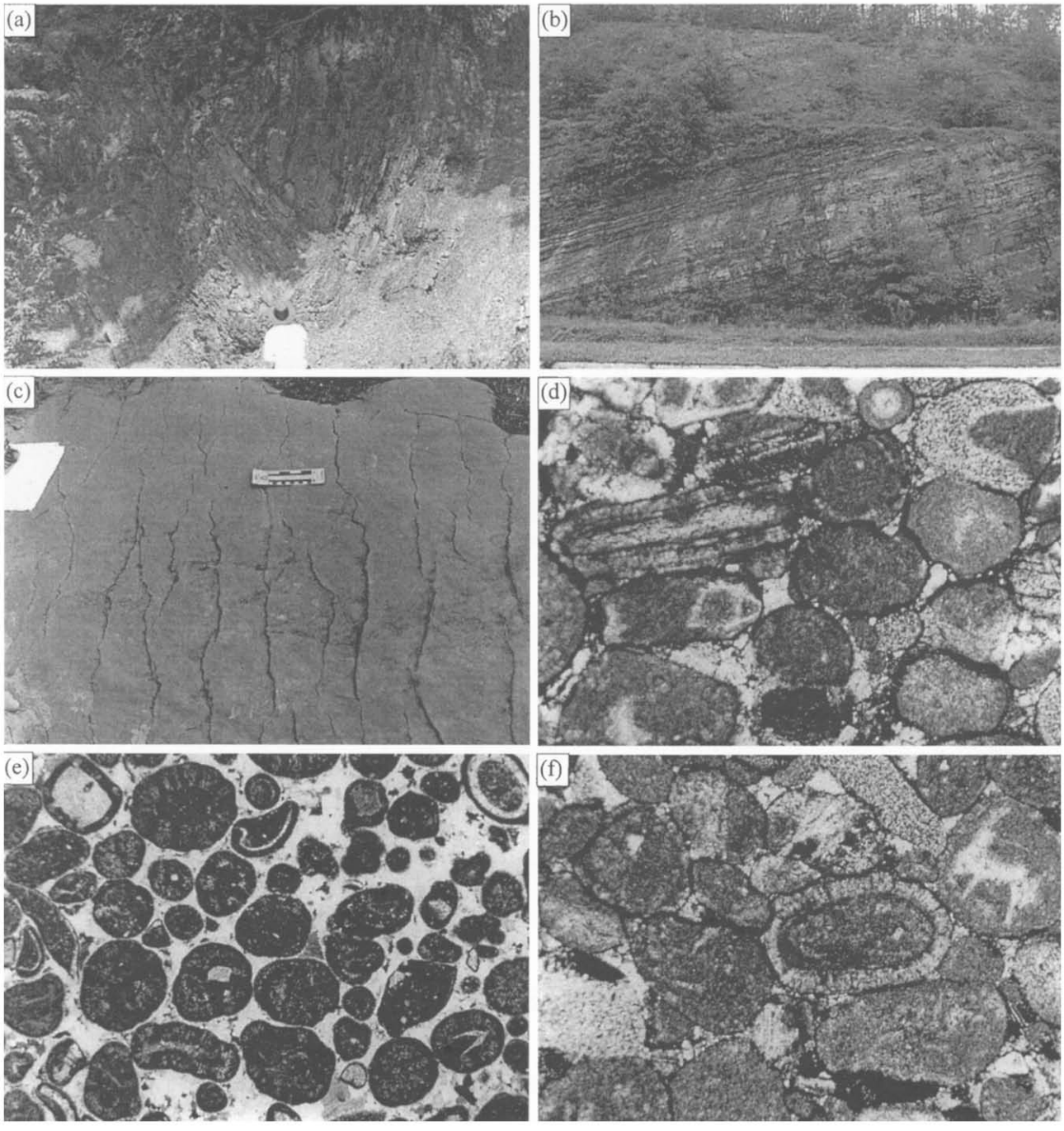

Fig. 5. (a) Intense folding of Devonian Brallier Formation in the core of Elkins Valley anticline. See line drawing in Fig. 6. (b) Uniformly SE-dipping Brallier Formation in the southeast limb of the Elkins Valley anticline. (c) Cleavage traces on a bedding surface of the Mississippian Greenbrier Group. (d) Bedding-perpendicular thin section showing Greenbrier grainstone with evidence of vertical compaction (field of view is 1.25 mm across). (e) Bedding-perpendicular thin section showing Greenbrier grainstone without evidence of vertical compaction (field of view is 5.0 mm across). (f) Bedding-parallel thin section of Greenbrier grainstone showing strike-parallel grain-to-grain solution (field of view is 1.25 mm across).

the study area (Figs 3 & 4). Examination of the many exposures reveals smooth changes in bedding dip that reflect the gentle open nature of the macroscale fold geometry (Fig. 4). Mesoscale folds and faults are almost completely absent in the Greenbrier Group. Thus, the dominant mesoscale structure in the Greenbrier Group (Fig. 5c and Appendix A) is a bedding-normal spaced, smooth-to-stylolitic disjunctive cleavage (Powell, 1979). Calculated bedding–cleavage dihedral angles are near 90° (Appendix A), which implies that cleavage was near-vertical if formed while bedding was horizontal.

Shortening estimates for the cleavage only in grainstones were obtained from scan lines perpendicular to cleavage traces on bedding. For each scan line, spacing between cleavage traces and average stylolite amplitude for each trace were recorded (Fig. 7). This technique

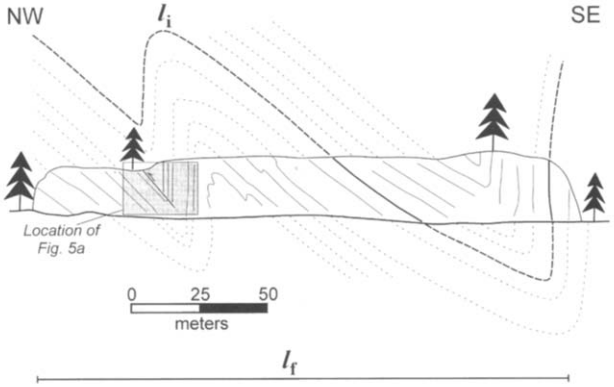

Fig. 6. Line sketch of a Brallier exposure in the core of the Elkins Valley anticline. Outcrop location is indicated on Fig. 3. l_i and l_f are the initial (undeformed) and final (deformed) line lengths, respectively. The location of Fig. 5(a) is also indicated.

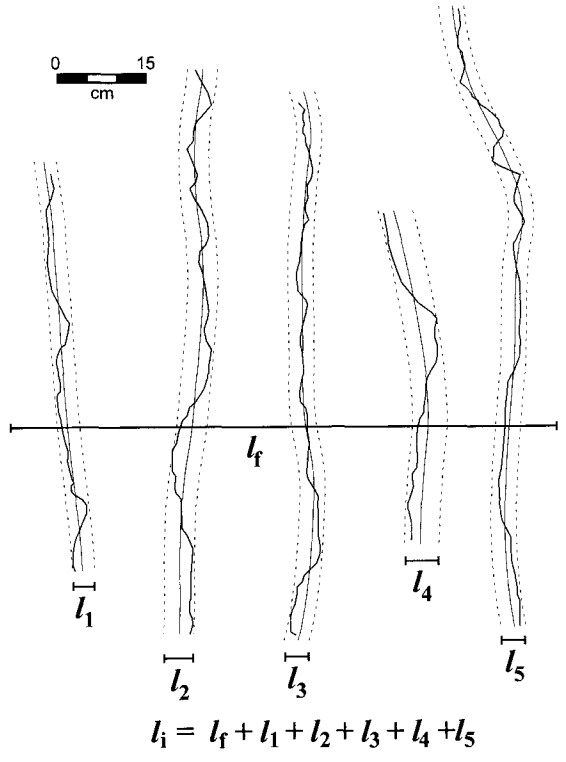

Fig. 7. Schematic representation of shortening measurement with a scan line from stylolitic cleavage traces on a bedding surface. l_f is the scan-line length and l_1–l_5 are the stylolite amplitudes for each cleavage trace. The scan line starts and ends in the middle of microlithons.

assumes that the amplitude of the stylolite teeth is approximately equal to the width of dissolved material, and as such this measurement represents a minimum shortening estimate because material may have been removed without increasing stylolite amplitude. This assumption of minimum shortening is a premise of the original solution explanation for stylolite formation (Stockdale, 1922, p. 59), is an explicit result of stylolite formation as anticracks (Fletcher and Pollard, 1981) and is consistent with an independent measure of strain vs size of stylolitic teeth (Alvarez *et al.*, 1978). Shortening was calculated as an elongation (Means, 1976, p. 133), where

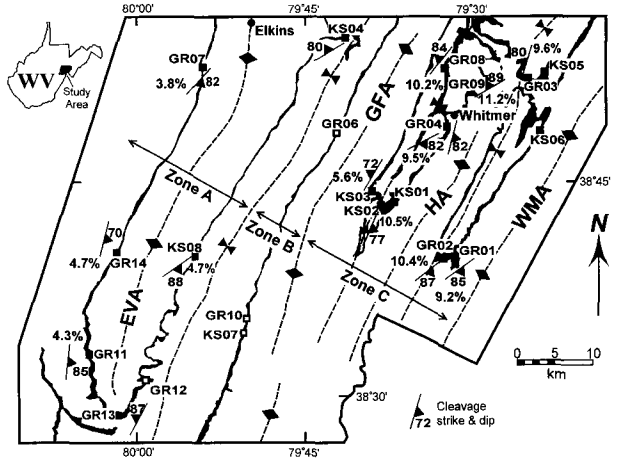

Fig. 8. Greenbrier Group cleavage map. The orientation of cleavage in grainstones and percent shortening values (where measured) are shown for solid squares. Open squares indicate sample locations without cleavage in grainstones.

the final length is the length of the scan line and the initial length is the final length plus the sum of the amplitudes of the stylolitic teeth (Fig. 7).

Cleavage-related layer-parallel shortening (Fig. 8 and Appendix A) is greatest in the eastern part of the area at 6–11%, decreases to near zero in the southeast limb of the North Potomac syncline and then increases across the Elkins Valley anticline to 4–5%. Intensity at three localities, GR01, GR02 and GR03 (Fig. 8 and Appendix A), was more difficult to estimate because the cleavage traces were smoothly undulating rather than the more typical stylolitic. Alvarez *et al.* (1978) noted that increased shortening is characterized by a transition from stylolitic to smooth surfaces because the wavelength of the teeth increases faster than the tooth amplitude. Consequently, the values at these localities should definitely be considered as minima.

The study area was divided into three zones (Fig. 8), based on the average cleavage intensity, so that the regional contribution to shortening by cleavage formation could be estimated. Zone A is 19.1 km wide, has a Greenbrier Group bed length of 19.7 km, average cleavage intensity of 4.4% and records 0.9 km of shortening. Zone B is 7.3 km wide, considered to lack cleavage and consequently records no shortening. Zone C is 22.9 km long, has a bed length of 25.4 km, an average intensity of 9.5% and records 2.4 km of shortening. Total shortening due to cleavage development is 3.3 km across the study area.

The change from a NW-decreasing shortening by cleavage to a greater cleavage-related shortening in the Elkins Valley anticline is interpreted to reflect two macroscale causes for the cleavage. To the north in Pennsylvania and New York (Engelder, 1979a,b; Engelder and Geiser, 1979; Geiser and Engelder, 1983) cleavage intensity typically decreases northwest away from the Wills Mountain anticline (Nittany anticlinorium) into the Plateau. This change is interpreted to result from decreased shortening by forethrusting in front of

the horses of the Cambro-Ordovician carbonates under the Wills Mountain anticline. The northwest decrease in intensity in the study area is consistent with this interpretation and is similarly interpreted, but the cleavage intensifies in the Elkins Valley anticline over the only horse of Cambro-Ordovician carbonates under the study area (Fig. 4b). This coincidence of geometry is interpreted to mean that cleavage intensification represents a local compensation response by the roof sequence.

Two different cleavage orientations, trending 020–030° and 050–060°, are present in the Greenbrier Group grainstones (Appendix A). Both orientations are only seen together at Station GR04 in a series of rock pavements to the south of Whitmer, West Virginia (GR04 in Fig. 8). The 020–030° surfaces terminate at the 050–060° surfaces. The 050–060°-trending surfaces possess oblique stylolitic teeth indicating a shortening direction of 110–120° rather than 140–150°. The 020–030°-trending surfaces have perpendicular stylolitic teeth yielding a shortening direction of 110–120°. A few minor contraction faults mutually offset, or are offset by, cleavage surfaces of both orientations, and have slickenlines trending 115°. The common shortening direction of the three sets of structures, their coeval deformation and the fact that 115° is the regional shortening direction (Rodgers, 1963, 1970; Gwinn, 1964; Perry, 1978; Geiser and Engelder, 1983) are used as evidence to interpret that all the structures were formed during one shortening event. A possible explanation is that a pre-existing anisotropy, such as a bedding-normal joint set (Geiser and Sansone, 1983), trending 050–060° was reactivated as solution surfaces while new structures, the 020–030°-trending cleavage and the contraction faults, formed. Extrapolating this interpretation to the entire study area, the two cleavage orientations do not represent two shortening directions but rather old and new structures accommodating a single shortening event.

Other workers in the central Appalachians (Dean *et al.*, 1988; Markley and Wojtal, 1996) have identified non-coaxial deformation where two or more cleavages formed. Our morphological observations and interpretation of a single deformation are consistent with their results. Dean *et al.* (1988) also examined stylolitic cleavage in the Greenbrier Group in an adjacent area to the south. Where they found evidence for non-coaxial deformation, stylolites in different orientations did not have parallel teeth and some older stylolites had teeth recording more than one shortening direction. These features were not found at GR04. In contrast, Dean *et al.* (1988) found multiple sets of stylolites with different surface orientations but parallel teeth. They interpreted the stylolites with the non-normal teeth to be joints reactivated as stylolites, as we have done. Markley and Wojtal (1996) found that each shortening event formed morphologically different cleavage, which is not the case at GR04 where all of the cleavage in the grainstones is stylolitic.

Of the 17.5 km of Cambro-Ordovician shortening, meso- and macroscale mechanisms (Table 1) accommodated 5.7 km at the Greenbrier level and 3.6 km at the Chemung level. This still leaves 11.8 km unaccounted for at the Greenbrier level and 13.9 km at the Chemung level.

MICROSCALE STRAIN ASSESSMENT

Deformed crinoids in the Chemung Group

Crinoid-bearing sandstones of the Devonian Chemung Group are exposed in the limbs and cores of the anticlines in the study area (Fig. 3). The total number of samples was limited because of the need to collect *in situ* oriented specimens, to have a sufficient number of crinoid columnals to calculate a representative shortening value and to have crinoid columnals parallel to bedding so layer-parallel shortening could be determined. A total of eight usable samples were collected (Fig. 3).

The axial ratio (R_f) of maximum and minimum columnal diameters and the orientation (ϕ) with respect to bedding strike of the maximum diameter were measured for at least 17 columnals in each sample. The harmonic mean of the R_f values (Lisle, 1977; Ramsay and Huber, 1983) was calculated as the best representation of the finite-strain ratio (R_s). A shortening estimate calculated from this strain value assumes that the crinoid columnal was initially circular, the harmonic mean of the R_f values represents the true finite-strain ellipse and the maximum columnal diameter remained undeformed (i.e. only the short axis changes length due to a net volume loss). Detailed observations of the crinoid columnals indicate that transgranular pressure solution played the major role in the observed shape change suggesting that most deformation was by volume loss. This interpretation is in agreement with studies of deformed crinoids in the Appalachian Plateau of New York and Pennsylvania (Engelder and Engelder, 1977; Engelder, 1979a; Engelder and Geiser, 1979; Oertel *et al.*, 1989).

Percent shortening was calculated for a case of volume loss (Onasch, 1984, p. 164). The eight crinoid-bearing samples of the Chemung Group yield layer-parallel shortening magnitudes of 9.1–16.7% with an average of $12.2 \pm 2.5\%$ (Appendix B). In contrast, Nair (1992) reported a shortening estimate of $17.2 \pm 2.6\%$ from one oriented and 45 unoriented Chemung Group samples in the Plateau of eastern West Virginia. The results differ between the two studies because Nair (1992) used the geometric mean of the R_f values as the strain ratio, which overestimates the strain ratio more than the harmonic mean (Lisle, 1977; Ramsay and Huber, 1983). The average strain ratio in Nair (1992) is 1.21 ± 0.04. The average strain ratio for our study recalculated with the geometric rather than harmonic mean is 1.19 ± 0.04, so consequently the results of the two studies are similar.

Shortening direction ranges from 090° to 147°, with an average of $118 \pm 17°$ (Appendix B). Because the short-

ening values are fairly uniform across the study area, the average shortening value of 12.2% for the 51.7 km bed length of the Chemung Group (Fig. 4b) indicates 6.3 km of shortening at this level by solution-related microscale deformation.

Calcite twin strains in the Greenbrier Group

Twenty-two oriented samples of ooid and crinoid grainstones were collected because they contain abundant markers for strain measurement techniques such as twin strain gauge, normalized Fry, and R_f/ϕ (Ramsay, 1967; Dunnet, 1969; Groshong, 1972, 1974; Groshong *et al.*, 1984a; Fry, 1979; Erslev, 1988; Schultz-Ela, 1990; Evans and Groshong, 1994). The calcite strain-gauge technique was used to calculate twinning strains in about 25 grains from each of two mutually perpendicular sections for 17 samples. Calculations used the inner twin width for thick twins and a twinned material ratio of 0.5 for thin twins (Groshong, 1974; Groshong *et al.*, 1984a; Evans and Groshong, 1994). Measurement precision and accuracy were improved by discarding 20% of the twin sets with the largest deviation from the calculated strain tensor, minimizing measurement errors and the effects of inhomogeneous deformation (Groshong, 1974; Groshong *et al.*, 1984a,b; Ferrill, 1991; Ferrill and Groshong, 1993a,b).

The total distortion for twinned samples varies from 0.1 to 4.2% and averages $1.3 \pm 1.0\%$ with no systematic regional variation in magnitude (Fig. 9 and Appendix C). Maximum shortening (ϵ_3) axes (Figs 9 & 10) mostly plunge gently east-southeast ($\sim 110°$) or west-northwest ($\sim 290°$). The maximum (ϵ_1) and intermediate (ϵ_2) axes form an 020°-trending, near-vertical girdle in which the maximum axes are more often steeply plunging. The average twin-related distortion of 1.3% for a Greenbrier bed length of 51.7 km (Fig. 4b) accommodates 0.7 km of shortening by twinning across the study area.

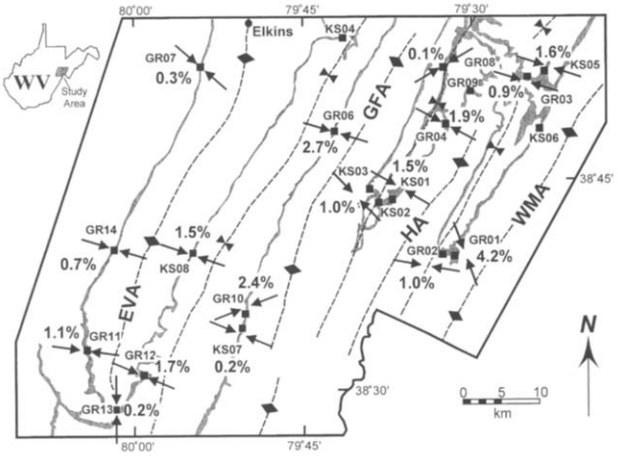

Fig. 9. Map of Greenbrier Group showing maximum shortening (ϵ_3) axes from the calcite strain-gauge technique (inward-pointing pairs of arrows). At each locality, the total distortion is also given as a percent shortening.

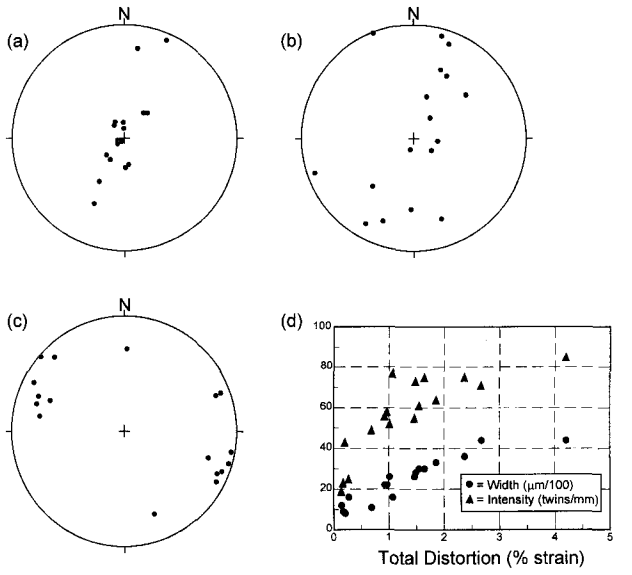

Fig. 10. Greenbrier Group calcite strain data. Equal-area lower-hemisphere plots of (a) long (ϵ_1), (b) intermediate (ϵ_2) and (c) short (ϵ_3) axes for 17 samples. (d) Relationship of the total distortion to average twin width (circles) and twin intensity (triangles).

The increase in twin intensity with total distortion is significantly greater than the increase in twin width (Fig. 10d). Thus, greater strain was accommodated by growth of new thin twins rather than by widening of existing twins during progressive deformation (Ferrill, 1991). This deformation behavior is consistent with conodont color alteration indices of 2.0–3.0 (Epstein *et al.*, 1977; Harris *et al.*, 1978, 1994) and a burial depth of less than 3 km for the Greenbrier Group, indicating temperatures of less than 200°C during deformation. Ferrill (1991) showed that increasing twin abundance rather than twin widening accommodates strain when the temperature is less than 170°C.

Finite-strain analyses in the Greenbrier

For the normalized Fry and R_f/ϕ methods (Ramsay, 1967; Dunnet, 1969; Fry, 1979; Erslev, 1988; Schultz-Ela, 1990) three mutually perpendicular thin sections were prepared from each of the 18 oriented samples. Grain boundaries in enlarged photomicrographs of each thin section were digitized as lines consisting of hundreds of points. Digitizing and strain calculations were performed using software developed by W. A. Yonkee (written communication, 1989). Finite-strain ellipses were determined for each section, and three-dimensional finite-strain ellipsoids were calculated from the three ellipses for each sample (Owens, 1984). As bedding dips are low, principal ellipsoidal axes are shown with bedding rotated to the horizontal to provide a common reference frame.

Bedding-perpendicular thin sections from 11 out of 18 samples from Greenbrier Group grainstones exhibit subhorizontal transgranular pressure-solution seams and sutured grain boundaries indicative of pre-tectonic vertical compaction. Consequently, the Greenbrier

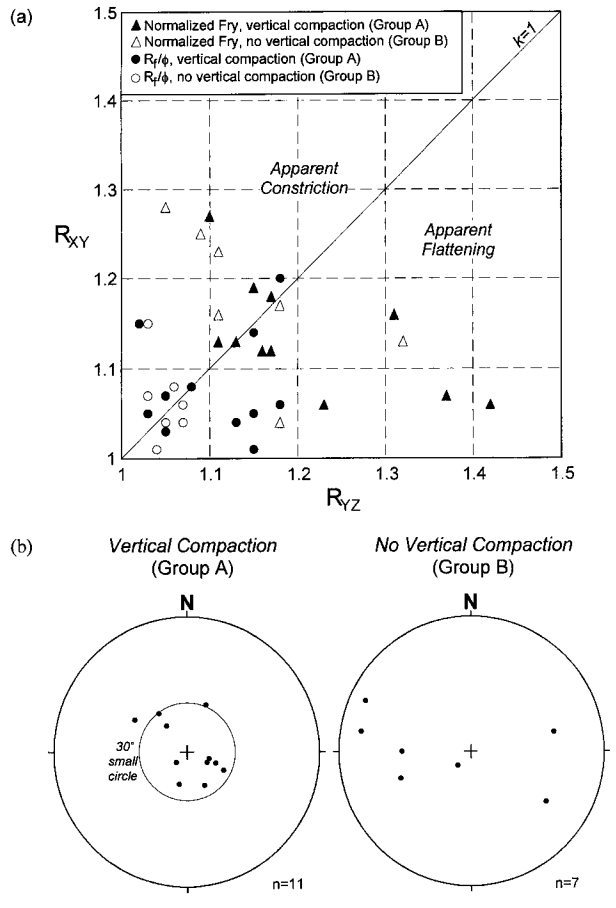

Fig. 11. Summary of Greenbrier finite-strain data. (a) Flinn graph of finite-strain ellipsoid axial ratios. (b) Equal-area lower-hemisphere projections of principal-strain ellipsoid short axes (Z) as determined from the normalized Fry method.

Group samples were divided into two groups: (1) Group A, evidence for vertical compaction (Fig. 5d); (2) Group B, no evidence of vertical compaction (Fig. 5e). Strain ratios from the normalized Fry method are similar for both groups and generally greater than R_f/ϕ strain ratios (Fig. 11a), whereas R_f/ϕ strain ratios for Group B samples are generally less than for Group A. Also, principal shortening (Z) axes determined by both techniques are more nearly vertical in the Group A samples (Fig. 11 and Appendices D and E). We interpret diagenetic compaction to produce the steeply plunging (subnormal to bedding) Z axes for both measurement techniques and the more elliptical, bedding-parallel grains that yield the increased strain ratios for the R_f/ϕ technique (Figs 5d & 11).

Assuming that pre-tectonic compaction was the typical uniaxial flattening with the short axis of the strain ellipsoid normal to bedding, bedding-parallel strain ellipses will remain circular after this early compactional event. As such, thin sections oriented parallel to bedding were analyzed for features indicative of deformation following the compaction event. Strike-parallel grain-to-grain sutures (Fig. 5f) and transgranular stylolites in the bedding-parallel sections of the Greenbrier Group grainstones indicate that pressure solution was the dominant deformation mechanism after compaction. Consequently, bedding-strain ellipses from the normalized Fry technique for vertically compacted samples were used to estimate the layer-parallel shortening in the Greenbrier Group (Appendix D). Strain ellipse axial ratios range from 1.03 to 1.22, and long axis trends range from 014 to 073°. Assuming volume loss, layer-parallel shortening ranges from 2.9 to 18.0% with an average of $10.7 \pm 4.9\%$, while the shortening direction ranges from 104° to 163° with an average of $135 \pm 17°$. The 10.7% average shortening over the bed length of 51.7 km is equivalent to 5.5 km of microscale shortening across the study area at the Greenbrier Group level.

DISCUSSION

Strain analyses at microscale through to macroscale demonstrate that only about two-thirds of the 17.5 km of blind thrust displacement of Cambro-Ordovician carbonates is accommodated in the Ordovician and younger roof sequence rocks of the study area (Table 1). The Ordovician and younger roof sequence rocks record about 10–12 km of shortening in the study area, however, indicating that forethrusting did play a fundamental role. Because the 17.5 km of displacement is not completely accommodated in the roof sequence in the study area, three explanations are possible: (1) backthrusting into the hinterland; (2) local compensation above the Wills Mountain duplex; or (3) more forethrusting beyond the study area. Of these alternatives backthrusting is least likely because the roof sequence above the Wills Mountain duplex lacks indicator features such as hinterland-vergent faults, asymmetric folds or cleavage (Thompson, 1979; Banks and Warburton, 1986; Dunne and Ferrill, 1988). The possibility of local compensation cannot be as easily discounted. Local compensation would require that the missing 5.6–7.6 km of shortening (15–22% shortening over the duplex) be accommodated in the roof sequence above the Wills Mountain duplex. This amount of shortening is typical of Silurian and Devonian rocks in the region (Ferrill and Dunne, 1989; Meyer and Dunne, 1990; Nair, 1992) and could be present above the duplex (Perry, 1975, 1978), however data are insufficient at present to reach a reliable conclusion. Nevertheless, the presence of shortening would not necessitate local compensation as it could be accommodating forethrusting by duplexes formed further into the hinterland.

Alternatively, forethrusting could be the dominant kinematic response if the missing displacement was transferred further into the Appalachian Plateau. Several lines of evidence suggest that additional forethrusting further into the Plateau has taken place. First, approximately 1.5 km of shortening at the Oriskany Sandstone level is present in a duplex under the Burning Springs anticline in northwestern West Virginia (Woodward, 1959; Calvert, 1983). Second, calcite twin strain measure-

ments in the Appalachian Plateau record 0.5–2% shortening as far as 400 km out in the Plateau (Craddock and Van der Pluijm, 1989; Craddock *et al.*, 1993; Van der Pluijm and Craddock, 1996). Assuming a conservative average of 1% over this distance yields 4 km of shortening in the Plateau. Finally, the Salina salt (Silurian), a well-documented décollement horizon in the Appalachian Plateau of western Pennsylvania and New York (Engelder, 1979a,b; Engelder and Engelder, 1977; Geiser and Engelder, 1983), is present in West Virginia from just northwest of the Elkins Valley anticline west to the Burning Springs anticline (Fig. 2). The Salina, because of its very low strength (Davis and Engelder, 1985), provides an ideal décollement horizon on which displacement can be transferred further into the foreland as forethrusting. Taken together, this evidence of additional shortening and active detachments further into the foreland is interpreted to mean that forethrusting dominated during emplacement of the Wills Mountain duplex.

As noted earlier, a large body of evidence has accumulated to document the role of forethrusting in accommodating Alleghanian blind thrusting in the Appalachian Plateau of Pennsylvania and New York where a salt décollement is present (Fig. 2) (Engelder and Engelder, 1977; Engelder, 1979a,b; Geiser and Engelder, 1983). Now that we have demonstrated a similar response along strike in West Virginia, where a salt décollement is absent, the question arises as to why the roof sequences behave the same way even though they do not share a common roof décollement. The different roof décollement horizons are the Silurian Salina salt in Pennsylvania and New York (Fig. 2) vs the Ordovician Martinsburg Formation in West Virginia (Fig. 4). One explanation for the similar behavior is that while a 'weak' décollement horizon in the foreland is a requirement for forethrusting (Smart *et al.*, 1997), a horizon containing salt may not be necessary. The fine-grained mudstones with some carbon content in the Martinsburg Formation (Wallace and Roen, 1989) may represent a sufficiently weak horizon for decoupling the Cambro-Ordovician carbonates from the overlying roof sequence (Wiltschko and Chapple, 1977; Byerlee, 1978; Jordan and Nüesch, 1989). Previous work also supports this possibility as: (1) the Martinsburg Formation is regionally extensive as a roof thrust (Kulander and Dean, 1986; Mitra, 1986; Wilson and Shumaker, 1988, 1992; Evans, 1989; Gray and Mitra, 1993; Onasch and Dunne, 1993; Dunne, 1996) from eastern Pennsylvania to southwestern Virginia, an area of over 15 000 km^2; and (2) forethrusting behavior has been documented elsewhere above this detachment (Ferrill and Dunne, 1989; Gray and Mitra, 1993).

A second explanation for the similarity in kinematic response may lie in the frontal geometry of the hangingwall ramp for the Wills Mountain duplex. The bedding above the ramp maintains a near-vertical orientation with an almost 90° cutoff against the roof detachment (Socolow, 1980; Herman, 1984; Kulander and Dean, 1986; Mitra, 1986; Wilson and Shumaker, 1988, 1992) that suggests that the duplex acted much like a bulldozer. The bedding in the roof sequence is also subvertical adjacent to the ramp (Fig. 4). This bedding geometry near the leading hangingwall ramp contrasts to a tapered-wedge shape (Fig. 12) for the frontal horses found in the Canadian Rockies (Thompson, 1979, 1982; Price, 1981; Jones, 1982; McMechan, 1985), the Sulaiman Range of Pakistan (Banks and Warburton, 1986; Humayon *et al.*, 1991; Jadoon *et al.*, 1994a,b) or the Subandean zone of Bolivia (Baby *et al.*, 1992), where dominant backthrusting behavior is inferred. For a 90°-dipping frontal bedding geometry the roof sequence rocks would have to translate directly up, against gravity, before they can displace towards the hinterland to achieve backthrusting or local compensation. Under these conditions it could be energetically less work to transfer duplex shortening into the foreland by forethrusting rather than towards the hinterland. Thus, the presence of this hangingwall geometry from Pennsylvania to Virginia in the Wills Mountain duplex could help to generate forethrusting through the roof sequence of the region.

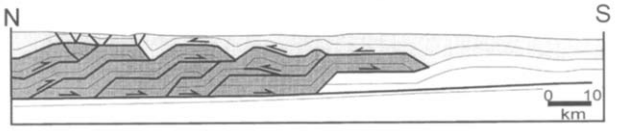

Fig. 12. Cross-section of the frontal and central Sulaiman fold belt, Pakistan. Modified from Jadoon *et al.* (1994a, fig. 4). Light gray, roof sequence; dark gray, blind 'tapered wedge'; arrows, slip directions of faults.

Lastly, the similarity in behavior could simply reflect a maintenance of strain compatibility between the foreland in Pennsylvania and New York and the foreland along strike in West Virginia. We do not favor this possibility because this strain compatibility requirement would be only a kinematic restriction with no clear underlying mechanical reason for existence. Mechanically, kinematic compatibility could be satisfied by different suites of structures, such as blind vs emergent thrusts, and would not require similar deformation styles as is actually found between the two regions.

In summary, we believe that the similar forethrusting behavior between the study area and previous work in the central Appalachians is the result of two different but similarly weak décollement horizons with a possible contribution from the geometry of the leading hangingwall ramp in the adjacent duplex.

This study demonstrates that approximately 75% of the roof sequence shortening occurred via mesoscale and smaller processes (Table 1). Of the 11.9 km of shortening recorded in the Greenbrier Group in the study area, microscale processes of grain-to-grain solution and twinning and mesoscale cleavage formation accounts for 80%. Only 2.4 km is taken up as macroscale folding. The Chemung Group accommodated 9.9 km of shortening of which 7.5 km (76%) is by microscale pressure solution and mesoscale folding and faulting. As with the

Greenbrier Group, macroscale folding in the Chemung Group accounts for only 2.4 km. Area calculations for the interval from the Martinsburg through to the Millboro Formations interval indicate that 15.3 km of shortening is accommodated by this interval of the roof sequence. Proprietary seismic reflection data demonstrate that much of this deformation occurs at less than macroscale. It is worth considering how a different conclusion might be reached if the micro- and mesoscale deformation was unmeasured in the Devonian and younger roof sequence. In this case, a large shortening imbalance (12.9 km or 84%) would occur between the Ordovician–Devonian and the Devonian–Mississippian parts of the roof sequence. Also, the upper roof sequence would show less shortening, requiring a detachment in the Devonian shales. Given the presence of significant deformation in the roof sequence above the Wills Mountain duplex (Perry, 1978), it would be reasonable to infer that the dominant kinematic response was local compensation or backthrusting. This interpretation would be incorrect and clearly demonstrates that all deformation scales need to be considered.

CONCLUSIONS

Kinematic analyses demonstrate that the roof sequence between Wills Mountain and the Elkins Valley anticline accommodates two-thirds of the 17.5 km of displacement from the Elkins Valley and Wills Mountain duplexes. Mesoscale and smaller processes including grain-to-grain pressure solution, twinning and cleavage formation account for over 75% of the shortening, with the remainder accommodated by macroscale folding and faulting.

The shortening magnitude suggests that forethrusting was the dominant kinematic response during duplex emplacement. The shortening imbalance between the Cambro-Ordovician section and the younger roof sequence rocks is accommodated by a combination of additional forethrusting further out in the foreland and local compensation above the duplexes.

This dominance by forethrusting is consistent with observations of forethrusting along strike in Pennsylvania and New York, despite a shift in the position of the roof detachment from shales in the Martinsburg Formation in the present study area to Silurian salt further north. We suggest that the similarity in response is due to the availability of a weak, albeit not salt, décollement and, possibly, the geometry of the leading hangingwall ramp for the Wills Mountain duplex with its near-vertical bedding and 90° cutoff angle.

The realization that micro- and mesoscale structures account for the majority (about 75%) of the deformation has important implications for workers in other tectonic systems. The absence of macroscale structures in the roof sequence forelandward of a blind thrust system is insufficient evidence for concluding that forethrusting is not the dominant kinematic response. As a consequence, accurate determination of the roof sequence response requires that deformation at all scales be evaluated.

Acknowledgements—Financial support for this project was provided to Kevin Smart by a research grant from the Geological Society of America, the Richard C. Hasson Memorial Grant from the American Association of Petroleum Geologists, a Grant-in-Aid of Research from Sigma Xi—The Scientific Research Society, a scholarship from the Mayo Educational Foundation and two research grants from the Department of Geological Sciences at The University of Tennessee. Bob Hatcher and Ken Walker improved the manuscript during its initial preparation. Reviews by Jim Evans, Mary Beth Gray and Mark McNaught significantly improved the final product.

REFERENCES

Adamson, G. W. (1992) Fold development in the cover enveloping the Broadtop horse. M.S. thesis, West Virginia University, Morgantown, U.S.A.

Alvarez, W., Engelder, T. and Geiser, P. A. (1978) Classification of solution cleavage in pelagic limestones. *Geology* **6**, 263–266.

Arkle, T., Jr (1974) Stratigraphy of the Pennsylvanian and Permian systems of the central Appalachians. In *Carboniferous of the Southeastern United States*, ed. G. Briggs, pp. 5–29. Special Paper of the Geological Society of America **148**.

Arkle, T., Beissel, D. R., Larese, R. E., Nuhfer, E. B., Patchen, D. G., Smosna, R. A., Gillespie, W. H., Lund, R., Norton, C. W. and Pfefferkorn, H. W. (1979) The Mississippian and Pennsylvanian (Carboniferous) system in the United States—West Virginia and Maryland. *Professional Paper of the United States Geological Survey* **1110D**, D1–D35.

Baby, P., Herail, G., Salinas, R. and Sempere, T. (1992) Geometry and kinematic evolution of passive roof duplexes deduced from cross section balancing: example from the foreland thrust system of the southern Bolivian Subandean zone. *Tectonics* **11**, 523–536.

Banks, C. J. and Warburton, J. (1986) 'Passive-roof' duplex geometry in the frontal structures of the Kirthar and Sulaiman mountain belts, Pakistan. *Journal of Structural Geology* **8**, 229–237.

Byerlee, J. D. (1978) Friction of rocks. *Pure and Applied Geophysics* **116**, 615–626.

Calvert, G. (1983) Subsurface structure of the Burning Springs anticline, West Virginia—Evidence for a two-stage structural development. *Proceedings of the Appalachian Basin Industrial Associates* **4**, 147–164.

Cardwell, D. H. (1982) *Oriskany and Huntersville Gas Fields of West Virginia*. West Virginia Geological and Economic Survey Mineral Report Series **MRS-5A**.

Cardwell, D. H., Erwin, R. B. and Woodward, H. P. (1968) *Geologic Map of West Virginia*, 1:250 000, 2 sheets. West Virginia Geological and Economic Survey.

Carney, C. K. (1987) Petrology and diagenesis of the upper Mississippian Greenbrier Limestone in the central Appalachian basin and of the lower Carboniferous Great Limestone in northern England. Ph.D. dissertation, West Virginia University, Morgantown, U.S.A.

Chamberlain, R. T. (1910) The Appalachian folds of central Pennsylvania. *Journal of Geology* **18**, 228–251.

Clifford, M. J. (1973) *Silurian Rock Salt of Ohio*. Ohio Geologic Survey Report of Investigations **90**.

Craddock, J. P. and Van der Pluijm, B. A. (1989) Late Paleozoic deformation of the cratonic carbonate cover of eastern North America. *Geology* **17**, 416–419.

Craddock, J. P., Jackson, M., Van der Pluijm, B. A. and Versical, R. T. (1993) Regional shortening fabrics in eastern North America: Far-field stress transmission from the Appalachian–Ouachita orogenic belt. *Tectonics* **12**, 257–264.

Dahlstrom, C. D. A. (1969) Balanced cross-sections. *Canadian Journal of Earth Sciences* **6**, 743–760.

Davis, D. M. and Engelder, T. (1985) The role of salt in fold-and-thrust belts. *Tectonophysics* **119**, 67–88.

Dean, S. L., Kulander, B. R. and Skinner, J. M. (1988) Structural chronology of the Alleghenian orogeny in southeast West Virginia. *Bulletin of the Geological Society of America* **100**, 299–310.

Dennison, J. M. and Naegele, O. D. (1963) *Structure of Devonian Strata Along the Alleghany Front From Corriganville, Maryland to Spruce Knob, West Virginia.* West Virginia Geological and Economic Survey Bulletin **24**.

De Paor, D. G. (1988) Balanced section in thrust belts, part 1: Construction. *Bulletin of the American Association of Petroleum Geologists* **72**, 73–90.

deWitt, W. and McGrew, L. W. (1979) Paleotectonic investigations of the Mississippian System in the United States—Appalachian basin region. *Professional Paper of the United States Geological Survey* **1010C**, 13–47.

Dunne, W. M. (1996) The role of macroscale thrusts in the deformation of the Alleghanian roof sequence in the central Appalachians: A re-evaluation. *American Journal of Science* **296**, 549–575.

Dunne, W. M. and Ferrill, D. A. (1988) Blind thrust systems. *Geology* **16**, 33–36.

Dunnet, D. (1969) A technique of finite strain analysis using elliptical particles. *Tectonophysics* **7**, 117–136.

Engelder, T. (1979) Mechanisms for strain within the Upper Devonian clastic sequence of the Appalachian Plateau, western New York. *American Journal of Science* **279**, 527–542.

Engelder, T. (1979) The nature of deformation within the outer limits of the central Appalachian foreland fold and thrust belt in New York State. *Tectonophysics* **55**, 289–310.

Engelder, T. and Engelder, R. (1977) Fossil distortion and decollement tectonics on the Appalachian Plateau. *Geology* **5**, 457–460.

Engelder, T. and Geiser, P. (1979) The relationship between pencil cleavage and lateral shortening within the Devonian section of the Appalachian Plateau, New York. *Geology* **7**, 460–464.

Epstein, A. G., Epstein, J. B. and Harris, L. D. (1977) Conodont color alteration—an index to organic metamorphism. *Professional Paper of the United States Geological Survey* **995**, 27 pp.

Erslev, E. A. (1988) Normalized center-to-center strain analysis of packed aggregates. *Journal of Structural Geology* **10**, 201–209.

Evans, M. A. (1989) The structural geometry and evolution of foreland thrust systems, northern Virginia. *Bulletin of the Geological Society of America* **101**, 339–354.

Evans, M. A. (1990) The structural geometry and evolution of foreland thrust systems, northern Virginia: Reply. *Bulletin of the Geological Society of America* **102**, 1444–1445.

Evans, M. A. (1997) Changes in pressure/temperature conditions in a deforming fold-and-thrust belt: central Appalachians. *Geological Society of America, Abstracts with Programs (southeast section)* **29**, A16.

Evans, M. A. and Dunne, W. M. (1991) Strain factorization and partitioning in the North Mountain thrust sheet, central Appalachians, U.S.A *Journal of Structural Geology* **13**, 21–35.

Evans, M. A. and Groshong, R. H. (1994) A computer program for the calcite strain-gauge technique. *Journal of Structural Geology* **16**, 277–281.

Ferrill, D. A. (1991) Calcite twin widths and intensities as metamorphic indicators in natural low-temperature deformation of limestone. *Journal of Structural Geology* **13**, 667–675.

Ferrill, D. A. and Dunne, W. M. (1989) Cover deformation above a blind duplex: An example from West Virginia, U.S.A. *Journal of Structural Geology* **11**, 421–431.

Ferrill, D. A. and Groshong, R. H. (1993) Kinematic model for the curvature of the northern Subalpine Chain, France. *Journal of Structural Geology* **15**, 523–541.

Ferrill, D. A. and Groshong, R. H. (1993) Deformation conditions in the northern Subalpine Chain, France, estimated from deformation modes in coarse-grained limestone. *Journal of Structural Geology* **15**, 995–1006.

Fletcher, R. C. and Pollard, D. D. (1981) Anticrack model for pressure solution surfaces. *Geology* **9**, 419–424.

Fry, N. (1979) Random point distributions and strain measurement in rock. *Tectonophysics* **60**, 89–105.

Geiser, P.A. (1988a) The role of kinematics in the construction and analysis of geological cross sections in deformed terranes. In *Geometries and Mechanisms of Thrusting, With Special Reference to the Appalachians*, eds G. Mitra and S. Wojtal, pp. 47–76. Special Paper of the Geological Society of America **222**.

Geiser, P. A. (1988) Mechanism of thrust propagation: some examples and implications for the analysis of overthrust terranes. *Journal of Structural Geology* **10**, 829–845.

Geiser, P. A. and Engelder, T. (1983) The distribution of layer parallel shortening fabrics in the Appalachian foreland of New York and Pennsylvania: Evidence for two non-coaxial phases of Alleghanian orogeny. In *Contributions to the Tectonics and Geophysics of Mountain Chains*, eds R. D. Hatcher, Jr, H. Williams and I. Zeitz, pp. 161–175. Memoir of the Geological Society of America **158**.

Geiser, P. A. and Sansone, S. (1983) Joints, microfractures, and the formation of solution cleavage in limestone. *Geology* **9**, 280–285.

Gray, M. B. and Mitra, G. (1993) Migration of deformation fronts during progressive deformation: evidence from detailed structural studies in the Pennsylvania Anthracite region, U.S.A. *Journal of Structural Geology* **15**, 435–449.

Groshong, R. H. (1972) Strain calculated from twinning in calcite. *Bulletin of the Geological Society of America* **83**, 2025–2038.

Groshong, R. H. (1974) Experimental test of least-squares strain gage calculation using twinned calcite. *Bulletin of the Geological Society of America* **85**, 1855–1864.

Groshong, R. H. and Epard, J.-L. (1992) Implications of area balance for strain and evolution of detachment folds. *Geological Society of America, Abstracts with Programs* **24**, A246.

Groshong, R. H. and Epard, J.-L. (1994) The role of strain in area-constant detachment folding. *Journal of Structural Geology* **16**, 613–618.

Groshong, R. H., Teufel, L. W. and Gasteiger, C. (1984) Precision and accuracy of the calcite strain-gage technique. *Bulletin of the Geological Society of America* **95**, 357–363.

Groshong, R. H., Pfiffner, O. A. and Pringle, L. R. (1984) Strain partitioning in the Helvetic thrust belt of eastern Switzerland from the leading edge to the internal zone. *Journal of Structural Geology* **6**, 5–18.

Gwinn, V. E. (1964) Thin-skinned tectonics in the Plateau and northwestern Valley and Ridge provinces of the central Appalachians. *Bulletin of the Geological Society of America* **75**, 863–900.

Harris, A. G., Harris, L. D. and Epstein, J. B. (1978) *Oil and Gas Data From Paleozoic Rocks in the Appalachian Basin: Maps For Assessing Hydrocarbon Potential and Thermal Maturity (Conodont Color Alteration Isograds and Overburden Isopachs)*, 1:2 500 000. United States Geological Survey Miscellaneous Investigations Series **I-917-E**.

Harris, A. G., Stamm, N. R., Weary, D. G., Repetski, J. E., Stamm, R. G. and Parker, R. A. (1994) *Conodont Color Alteration Index (CAI) Map and Conodont-based Age Determinations For the Winchester 30′ × 60′ Quadrangle and Adjacent Area, Virginia, West Virginia, and Maryland*, 1:100 000. United States Geological Survey Miscellaneous Field Studies Map **MF-2239**.

Herman, G. C. (1984) A structural analysis of a portion of the Valley and Ridge province of Pennsylvania. M.S. thesis, University of Connecticut, Storrs, U.S.A.

Humayon, M., Lillie, R. J. and Lawrence, R. D. (1991) Structural interpretation of the eastern Sulaiman foldbelt and foredeep, Pakistan. *Tectonics* **10**, 299–324.

Jadoon, I. A. K., Lawrence, R. D. and Khan, S. H. (1994) Mari-Bugti pop-up zone in the central Sulaiman fold belt, Pakistan. *Journal of Structural Geology* **16**, 147–158.

Jadoon, I. A. K., Lawrence, R. D. and Lillie, R. J. (1994) Seismic data, geometry, evolution, and shortening in the active Sulaiman fold-and-thrust belt of Pakistan, southwest of the Himalayas. *Bulletin of the American Association of Petroleum Geologists* **78**, 758–774.

Jones, P. B. (1982) Oil and gas beneath east-dipping underthrust faults in the Alberta Foothills, Canada. In *Geologic Studies of the Cordilleran Thrust Belt*, ed. R. B. Powers. *Rocky Mountain Association of Petroleum Geologists* **1**, 61–74.

Jordan, P. and Nüesch, R. (1989) Deformational behavior of shale interlayers in evaporite detachment horizons, Jura overthrust, Switzerland. *Journal of Structural Geology* **11**, 859–871.

Kulander, B. R. and Dean, S. L. (1986) Structure and tectonics of central and southern Appalachian Valley and Ridge and Plateau Provinces, West Virginia and Virginia. *Bulletin of the American Association of Petroleum Geologists* **70**, 1674–1684.

Lisle, R. J. (1977) Estimation of tectonic strain ratio from the mean shape of deformed elliptical markers. *Geologie en Mijnbouw* **56**, 140–144.

Markley, M. and Wojtal, S. (1996) Mesoscopic structure, strain, and volume loss in folded cover strata, Valley and Ridge Province, Maryland. *American Journal of Science* **296**, 23–57.

McMechan, M. E. (1985) Low-taper triangle-zone geometry: An interpretation for the Rocky Mountain foothills, Pine Pass–Peace River area, British Columbia. *Bulletin of Canadian Petroleum Geology* **33**, 31–38.

McNaught, M. A. and Mitra, G. (1996) The use of finite strain data in constructing a retrodeformable cross-section of the Meade thrust sheet, southeastern Idaho, U.S.A. *Journal of Structural Geology* **18**, 573–583.

Means, W. D. (1976) *Stress and Strain: Basic Concepts in Continuum Mechanics for Geologists*. Springer, New York.

Meyer, T. J. and Dunne, W. M. (1990) Deformation of Helderberg Limestones above the blind thrust system of the central Appalachians. *Journal of Geology* **98**, 108–117.

Mitra, G. (1994) Strain variation in thrust sheets across the Sevier fold-and-thrust belt (Idaho–Utah–Wyoming): implications for section restoration and wedge taper evolution. *Journal of Structural Geology* **16**, 585–602.

Mitra, G. and Yonkee, W. A. (1985) Relationship of spaced cleavage to folds and thrusts in the Idaho–Utah–Wyoming thrust belt. *Journal of Structural Geology* **7**, 361–373.

Mitra, S. (1986) Duplex structures and imbricate thrust systems: Geometry, structural position, and hydrocarbon potential. *Bulletin of the American Association of Petroleum Geologists* **70**, 1087–1112.

Mitra, S. and Namson, J. S. (1990) Equal-area balancing. *American Journal of Science* **289**, 563–599.

Morley, C. K. (1986) A classification of thrust fronts. *Bulletin of the American Association of Petroleum Geologists* **70**, 12–25.

Morley, C. K. (1987) Lateral and vertical changes of deformation style in the Osen–Roa thrust sheet, Oslo Region. *Journal of Structural Geology* **9**, 331–343.

Nair, N. S. (1992) Crinoid deformation and regional structural geology in eastern West Virginia and northwestern Virginia. M.S. thesis, University of Toledo, Toledo, U.S.A.

Oertel, G., Engelder, T. and Evans, K. (1989) A comparison of the strain of crinoid columnals with that of their enclosing silty and shaly matrix on the Appalachian Plateau, New York. *Journal of Structural Geology* **11**, 975–993.

Onasch, C. M. (1984) Application of the R_f/ϕ technique to elliptical markers deformed by pressure-solution. *Tectonophysics* **110**, 157–165.

Onasch, C. M. and Dunne, W. M. (1993) Variation in quartz arenite deformation mechanisms between a roof sequence and duplexes. *Journal of Structural Geology* **15**, 465–475.

Owens, W. H. (1984) The calculation of a best-fit ellipsoid from elliptical sections on arbitrarily oriented planes. *Journal of Structural Geology* **6**, 571–578.

Patchen, D. G., Kline, P. C., Patchen, M. A., Cardwell, D. H. and Behling, M. C. (1977) *Catalog of Subsurface Information for West Virginia*. West Virginia Geological and Economic Survey Mineral Resources Series **6**.

Perry, W. J. (1975) Tectonics of the western Valley and Ridge foldbelt, Pendleton County, West Virginia—A summary report. *United States Geological Survey Journal of Research* **3**, 583–588.

Perry, W. J. (1978) Sequential deformation in the central Appalachians. *American Journal of Science* **278**, 518–542.

Powell, C. McA. (1979) A morphological classification of rock cleavage. *Tectonophysics* **58**, 21–34.

Price, P. H. (1929) *Pocahontas County*, 2 maps. West Virginia Geological and Economic Survey.

Price, P. H. and Heck, E. T. (1939) *Greenbrier County*, 2 maps. West Virginia Geological and Economic Survey.

Price, R. A. (1981) The Cordilleran foreland thrust and fold belt in the southern Canadian Rocky Mountains. In *Thrust and Nappe Tectonics*, eds K. R. McClay and N. J. Price, pp. 427–448. Geological Society of London Special Publication **9**.

Protzman, G. M. and Mitra, G. (1990) Strain fabric associated with the Meade thrust sheet: implications for cross-section balancing. *Journal of Structural Geology* **12**, 403–417.

Ramsay, J. G. (1967) *Folding and Fracturing of Rocks*. McGraw-Hill, New York.

Ramsay, J. G. and Huber, M. I. (1983) *The Techniques of Modern of Structural Geology, Volume 1: Strain Analysis*. Academic Press, London.

Reger, D. B. (1931) *Randolph County*, 2 maps. West Virginia Geological and Economic Survey.

Rodgers, J. (1963) Mechanics of Appalachian foreland folding in Pennsylvania and West Virginia. *Bulletin of the American Association of Petroleum Geologists* **47**, 1527–1536.

Rodgers, J. (1970) *The Tectonics of the Appalachians*. John Wiley and Sons, New York.

Schultz-Ela, D. D. (1990) A method of estimating errors in calculated strains. *Journal of Structural Geology* **12**, 939–943.

Smart, K. J., Couzens, B. A., Dunne, W. M. and Krieg, R. D. (1997) Kinematic behavior and structural geometry of thrust systems: Comparison of numerical and analog models. *Geological Society of America, Abstract with Programs (southeast section)* **29**, A–70.

Smosna, R. A. and Patchen, D. G. (1978) Silurian evolution of central Appalachian basin. *West Virginia Geological and Economic Survey Report of Investigations* **RI-29**, 2308–2328.

Smosna, R. A., Patchen, D. G., Warshauer, S. M. and Perry, W. J. (1978) Relationship between depositional environments, Tonoloway Limestone, and distribution of evaporites in the Salina Formation, West Virginia. *West Virginia Geological and Economic Survey Report of Investigations* **RI-28**, 125–143.

Socolow, A. A. (1980) *Geologic Map of Pennsylvania*, 1:250 000, 2 sheets. Pennsylvania Topographic and Geologic Survey,

Stockdale, P. B. (1922) *Styolites; their nature and origin*. Indiana University Studies, Birmingham, **9**, 97 pp.

Suppe, J. (1983) Geometry and kinematics of fault-bend folding. *American Journal of Science* **283**, 684–721.

Thompson, R. I. (1979) A structural interpretation across part of the northern Rocky Mountains, British Columbia, Canada. *Canadian Journal of Earth Sciences* **16**, 1228–1241.

Thompson, R. I. (1982) The nature and significance of large 'blind' thrusts within the northern Rocky Mountains of Canada. In *Geologic Studies of the Cordilleran Thrust Belt*, ed. R. B. Powers. Rocky Mountain Association of Geologists **1**, 47–59.

Tilton, J. L., Prouty, W. F. and Price, P. H. (1927) *Pendleton County*, 2 maps. West Virginia Geological and Economic Survey.

Van der Pluijm, B. A. and Craddock, J. P. (1996) Orogens as 'stress filters': Calcite twinning analysis in cratonic North America. *Geological Society of America, Abstracts with Programs* **28**, A187–A188.

Vann, I. R., Graham, R. H. and Hayward, A. B. (1986) The structure of mountain fronts. *Journal of Structural Geology* **8**, 215–227.

Wallace, L. G. and Roen, J. B. (1989) Petroleum source rock potential of the Upper Ordovician black shale sequence, northern Appalachian basin. *United States Geological Survey Open File Report* **89-488**, 66.

Wallace, W. K. and Hanks, C. L. (1990) Structural provinces of the northeastern Brooks Range, Arctic National Wildlife Refuge, Alaska. *Bulletin of the American Association of Petroleum Geologists* **74**, 1110–1118.

Wilson, T. H. and Shumaker, R. C. (1988) Three-dimensional structural interrelationships within Cambrian–Ordovician lithotectonic unit of central Appalachians. *Bulletin of the American Association of Petroleum Geologists* **72**, 600–614.

Wilson, T. H. and Shumaker, R. C. (1992) Broad Top thrust sheet: an extensive blind thrust in the central Appalachians. *Bulletin of the American Association of Petroleum Geologists* **76**, 1310–1324.

Wiltschko, D. V. and Chapple, W. M. (1977) Flow of weak rocks in Appalachian Plateau Folds. *Bulletin of the American Association of Petroleum Geologists* **61**, 180–197.

Woodward, H. P. (1941) *Silurian System of West Virginia*. West Virginia Geological Survey **XIV**.

Woodward, H. P. (1943) *Devonian System of West Virginia*. West Virginia Geological Survey **XV**.

Woodward, H. P. (1949) *Cambrian System of West Virginia*. West Virginia Geological Survey **XX**.

Woodward, H. P. (1951) *Ordovician System of West Virginia*. West Virginia Geological Survey **XXI**.

Woodward, H. P. (1959) Structural interpretations of the Burning Springs anticline. In *The Sandhill Deep Well, Wood County, West Virginia*, ed. H. P. Woodward. West Virginia Geological and Economic Survey Report Investigations **18**, 159–168.

Woodward, N. B., Boyer, S. E. and Suppe, J. (1989) *Balanced Geological Cross-sections: An Essential Technique in Geological Research and Exploration*. American Geophysical Union Short Course in Geology **6**.

Wu, S. (1993) Fractal strain distribution and its implications for cross-section balancing. *Journal of Structural Geology* **15**, 1497–1507.

APPENDIX A

The Greenbrier grainstone cleavage data are given in Table 2.

Table 2

Sample No.	Bedding orientation	Cleavage orientation		Bedding–cleavage dihedral angle (°)	Percent shortening‡
		Unrotated*	Rotated†		
GR01	063°/06°N	056°/85°S	056°/89°N	89	9.2
GR02	116°/04°S	053°/87°S	053°/89°S	85	10.4
GR03	014°/27°S	011°/80°N	011°/73°S	83	9.6
GR04	019°/12°N	064°/82°S	063°/90°	89	9.5
GR07	016°/12°N	040°/79°S	039°/90°	90	3.8
GR08	017°/07°S	040°/84°N	040°/90°	89	10.2
GR09	028°/05°N	061°/89°N	061°/85°N	87	11.2
GR11	004°/15°N	007°/85°S	007°/80°N	80	4.3
GR13	037°/07°S	030°/87°N	030°/86°S	86	n.a.§
GR14	018°/19°N	015°/70°S	015°/89°S	90	4.7
KS02	074°/19°N	024°/77°S	026°/89°S	90	10.5
KS03	017°/18°S	032°/72°N	031°/90°	90	5.6
KS04	083°/05°S	058°/82°N	058°/87°N	85	n.a.§
KS08	041°/13°S	057°/88°S	058°/75°S	76	4.7

*Present cleavage orientation.
†Cleavage orientation with bedding rotated to horizontal.
‡Minimum estimate (see text for details).
§Insufficient traces for shortening measurement.
n.a., not applicable.

APPENDIX B

The Chemung Group shortening data from deformed crinoids are given in Table 3.

Table 3

Sample No.	Bedding orientation	Harmonic mean of R_f	Mean ϕ trend*	Shortening direction†	Percent shortening
CH1	035°/18°N	1.10±0.10	033°±19°	123°	9.1
CH2	075°/13°N	1.16±0.14	057°±17°	147°	13.8
CH3	032°/16°S	1.12±0.09	012°±13°	102°	10.7
CH5	029°/22°S	1.20±0.11	032°±16°	122°	16.7
CH6	012°/19°S	1.12±0.09	000°±13°	090°	10.7
CH7	008°/14°N	1.12±0.05	026°±7°	116°	10.7
CH8	025°/20°S	1.12±0.12	043°±38°	133°	10.7
CH9	020°/20°N	1.18±0.11	020°±20°	110°	15.3
			Average	118°±17°	12.2±2.5

*Orientation of the long axis of crinoid columnal after bedding rotated to horizontal.
†Calculated as perpendicular to the mean ϕ trend.

APPENDIX C

The Greenbrier Group twin strain data are given in Table 4.

Table 4

Sample (bedding)	Cleaning procedure*	No. of twin sets	Principal strains (% elongation)			Principal axis orientations with bedding horizontal			Nominal error in strain	% NEV	Average twin width (μm)	Average twin intensity (twins/mm)	Total distortion (% strain)
			ϵ_1	ϵ_2	ϵ_3	ϵ_1	ϵ_2	ϵ_3					
GR01	n.a.	49	3.73	−0.47	−3.33	309/84	076/04	166/05	0.59	55.1	0.51	94	3.52
063/06N	LDR	40	4.14	0.44	−3.70	346/79	251/01	161/11	0.50	30.0	0.44	77	3.94
GR02	n.a.	48	1.31	0.04	−1.36	032/57	186/30	283/12	0.22	12.5	0.31	56	1.33
331/06N	LDR	39	1.03	−0.04	−0.99	038/59	182/26	280/16	0.15	20.5	0.26	52	1.02
GR03	n.a.	50	2.19	−0.63	−1.56	188/68	028/21	295/07	0.42	20.0	0.33	63	1.95
024/32S	LDR	40	1.02	−0.25	−0.77	172/63	022/24	287/12	0.14	20.0	0.22	56	0.92
GR04	n.a.	49	1.74	0.84	−2.58	330/86	210/02	120/03	0.34	14.3	0.42	67	2.28
019/12N	LDR	40	1.23	0.91	−2.14	355/80	209/08	118/05	0.29	10.0	0.33	64	1.86
GR05	n.a.	48	0.19	0.07	−0.26	197/80	338/09	069/07	0.04	6.3	0.19	22	0.23
017/10S	LDR	39	0.11	0.05	−0.16	246/82	339/00	069/08	0.03	5.1	0.12	19	0.14
GR06	n.a.	49	2.90	2.46	−5.37	020/34	203/56	111.01	1.61	12.2	0.68	74	4.65
030/18N	LDR	40	2.14	0.86	−3.00	228/85	016/04	107/02	0.62	15.0	0.44	71	2.68
GR07	n.a.	50	0.38	0.15	−0.53	075/70	221/18	315/10	0.13	18.4	0.24	29	0.47
025/19N	LDR	40	0.22	0.09	−0.31	043/57	221/32	311/01	0.06	7.5	0.16	25	0.27
GR10	n.a.	46	4.66	−1.06	−3.60	303/71	169/13	076/13	0.94	15.2	0.49	91	4.23
043/16N	LDR	37	2.37	0.00	−2.37	323/73	160/16	069/05	0.54	10.8	0.36	75	2.37
GR11	n.a.	48	1.46	0.37	−1.83	008/05	172/84	278/01	0.25	16.7	0.25	85	1.67
004/15N	LDR	39	0.97	0.19	−1.15	009/13	198/78	11/02	0.15	15.4	0.16	77	1.07
GR12	n.a.	49	1.78	0.88	−2.66	048/59	195/27	293/15	0.31	22.4	0.39	76	2.35
027/11S	LDR	40	1.10	0.80	−1.90	024/04	124/69	292/20	0.20	15.0	0.30	75	1.65
GR13	n.a.	50	0.38	0.10	−0.48	202/73	083/09	351/15	0.11	34.0	0.15	46	0.44
037/07S	LDR	40	0.15	0.09	−0.24	226/65	097/65	002/19	0.05	27.5	0.08	43	0.21
GR14	n.a.	50	0.97	0.02	−0.99	333/66	198/18	102/16	0.16	12.0	0.20	51	0.94
018/19N	LDR	40	0.69	−0.01	−0.69	329/71	200/14	107/14	0.11	7.5	0.11	49	0.69
KS01	n.a.	49	2.42	−0.30	−2.12	217/72	028/18	119/03	0.39	22.5	0.44	59	2.28
007/17N	LDR	40	1.62	−0.04	−1.58	215/57	024/33	117/05	0.23	30.0	0.30	51	1.60
KS03	n.a.	50	1.67	−0.15	−1.53	191/73	043/15	311/09	0.22	8.0	0.31	67	1.61
017/18N	LDR	40	0.96	0.01	−0.97	214/64	050/28	316/07	0.13	17.5	0.20	58	0.97
KS05	n.a.	45	1.61	0.20	−1.82	243/89	030/01	120/01	0.48	28.9	0.42	60	1.73
045/09S	LDR	36	1.28	0.44	−1.72	205/25	040/64	298/06	0.35	19.4	0.30	61	1.55
KS07	n.a.	44	0.31	0.03	−0.34	184/67	024/24	290/28	0.07	18.2	0.18	26	0.33
036/20N	LDR	36	0.19	−0.02	−0.16	179/61	028/26	292/12	0.04	13.9	0.09	23	0.18
KS08	n.a.	50	1.40	0.99	−2.31	343/81	204/06	113/05	0.25	22.0	0.38	84	2.08
041/13S	LDR	40	0.88	0.83	−1.72	229/81	021/07	112/04	0.20	17.5	0.28	73	1.49

*LDR, 20% of largest deviations removed; n.a., not applicable.

APPENDIX D

The Greenbrier Group finite-strain data from the normalized Fry technique are given in Table 5.

Table 5

Sample No.	Group*	Bedding orientation	Principal axes†			Axial ratios		Bedding-parallel strain data		
			X	Y	Z	R_{XY}	R_{YZ}	R_S	Percent shortening	Shortening direction
KS02	A	074°/19°N	180°/23°	084°/15°	323°/61°	1.27	1.10	1.20	16.7	133°
KS03	A	017°/18°S	009°/18°	276°/13°	152°/67°	1.12	1.17	1.08	7.4	104°
KS04	A	083°/05°S	068°/12°	335°/16°	194°/70°	1.19	1.15	1.18	15.3	163°
KS06	A	019°/20°N	338°/03°	069°/08°	224°/81°	1.13	1.13	1.11	9.9	154°
KS08	A	041°/13°S	209°/08°	117°/19°	321°/70°	1.06	1.42	1.12	10.7	133°
GR02	A	331°/06°N	214°/31°	120°/05°	022°/59°	1.16	1.31	1.03	2.9	151°
GR04	A	019°/12°N	207°/03°	298°/19°	111°/71°	1.07	1.37	1.12	10.7	114°
GR05	A	017°/10°S	350°/36°	250°/13°	114°/76°	1.12	1.16	1.03	2.9	137°
GR06	A	030°/19°N	183°/21°	080°/30°	301°/52°	1.06	1.23	1.22	18.0	120°
GR07	A	025°/19°N	272°/14°	004°/04°	111°/76°	1.27	1.14	1.10	9.1	150°
GR12	A	027°/11°S	210°/01°	300°/25°	117°/65°	1.13	1.11	1.17	14.5	125°
KS05	B	045°/09°S	348°/49°	229°/23°	124°/33°	1.28	1.05			
GR01	B	063°/06°N	007°/07°	104°/44°	270°/46°	1.25	1.09			
GR03	B	014°/27°S	351°/12°	093°/46°	250°/42°	1.17	1.18			
GR10	B	043°/16°N	175°/41°	026°/44°	280°/16	1.04	1.18			
GR11	B	004°/15°N	242°/53°	342°/07°	077°/36°	1.23	1.11			
GR13	B	037°/07°S	063°/12°	332°/03°	224°/78	1.13	1.32			
GR14	B	018°/19°N	183°/60°	032°/27°	295°/12°	1.16	1.11			

*Group A, vertical compaction; Group B, no vertical compaction.
†Principal-strain axis orientations with bedding rotated to the horizontal.

APPENDIX E

The Greenbrier Group finite-strain data from the R_f/ϕ technique are given in Table 6.

Table 6

Sample No.	Group*	Bedding orientation	Principal axes†			Axial ratios	
			X	Y	Z	R_{XY}	R_{YZ}
KS02	A	074°/19°N	209°/25°	308°/18°	070°/59°	1.15	1.02
KS03	A	017°/18°S	298°/23°	204°/08°	098°/66°	1.01	1.15
KS04	A	083°/05°S	185°/29°	090°/08°	345°/59°	1.05	1.15
KS06	A	019°/20°N	164°/06°	255°/06°	030°/82°	1.08	1.08
KS08	A	041°/13°S	217°/17°	309°/08°	063°/72°	1.20	1.18
GR02	A	331°/06°N	223°/28°	121°/23°	358°/53°	1.04	1.13
GR04	A	019°/12°N	014°/02°	103°/02°	226°/87°	1.06	1.18
GR05	A	017°/10°S	090°/03°	182°/20°	350°/70°	1.05	1.03
GR06	A	030°/19°N	204°/17°	109°/18°	338°/65°	1.07	1.05
GR07	A	025°/19°N	255°/33°	156°/14°	047°/54°	1.14	1.15
GR12	A	027°/11°S	076°/03°	347°/01°	243°/87°	1.03	1.05
KS05	B	045°/09°S	034°/16°	254°/70°	128°/12°	1.01	1.04
GR01	B	063°/06°N	034°/15°	302°/10°	179°/71°	1.14	1.03
GR03	B	014°/27°S	012°/10°	103°/03°	214°/79°	1.03	1.07
GR10	B	043°/16°N	082°/06°	188°/68°	350°/21°	1.04	1.05
GR11	B	004°/15°N	245°/54°	005°/20°	106°/29°	1.08	1.06
GR13	B	037°/07°S	179°/06°	269°/02°	021°/85°	1.07	1.03
GR14	B	018°/19°N	001°/07°	267°/26°	105°/63°	1.06	1.07

*Group A, vertical compaction; Group B, no vertical compaction.
†Principal strain axis orientations with bedding rotated to the horizontal.